

A numerical study on the formation of the Kuroshio Counter Current and the Kuroshio Branch Current in the East China Sea

Bo QIU* and NORIHISA IMASATO*

(Received 25 September 1987; in revised form 20 April 1989; accepted 21 August 1989)

Abstract—The Kuroshio Counter Current (KCC) and the Kuroshio Branch Current (KBC) are two unique features of the Kuroshio in the East China Sea. The mechanisms that generate the KCC and the KBC are studied using a barotropic inflow–outflow model with a simplified basin configuration of the East China Sea. The present study shows that the KCC can only exist on a β -plane frame of reference and its flow pattern is independent of the offshore Ryukyu Islands. In the East China Sea, the continental slope plays the role of a western boundary for the Kuroshio. Whether the Kuroshio protrudes onto the slope region, however, is found to have little influence on the KCC. Concerning the formation of the KBC, we found that the planetary β -effect and the existence of Taiwan Island are two indispensable conditions: the planetary β -effect drives part of the Kuroshio inflow to branch southwestward and Taiwan Island blocks this branched current causing it to protrude onto the continental shelf. Based on the numerical calculation, we further found that the branch current is reinforced by topographic Rossby waves induced by the repeated crossing of the Kuroshio over the continental slope.

1. INTRODUCTION

THE Kuroshio originates in the North Equatorial Current and flows into the East China Sea through the passage between Taiwan and Yonakuni-jima, an island at the southwestern tip of the Ryukyu Islands. Under the constraint of the steep continental slope, the main stream of the Kuroshio in the East China Sea runs stably along the 200 m isobath at a maximum velocity of 75–150 cm s⁻¹ (NITANI, 1972). After it turns eastward around 30°29'N latitude and 129°E longitude, the Kuroshio eventually flows out into the Pacific through the Tokara Strait.

Figure 1 shows schematically the Kuroshio's flow pattern in the East China Sea. Notice that a counter current flowing southwestward exists between the main stream of the Kuroshio and the Ryukyu Islands. The observational evidence of the Kuroshio Counter Current (KCC) was obtained both from the movement of drifter bottles during winter in the East China Sea (KONDO and TAMAI, 1975) and from direct CTD and GEK measurements. Figure 2 shows geostrophic velocity profiles calculated by INOUE (1981) from the CTD measurements along the PN section (see Fig. 1 for its location). The KCC, as indicated by the offshore shaded regions, has a maximum speed ranging from 20 to 50 cm s⁻¹ and its volume transport tends to weaken in autumn. This tendency is possibly related to the fact that the Kuroshio in the East China Sea has a smaller volume transport in

*Geophysical Institute, Kyoto University, Kyoto, 606 Japan.

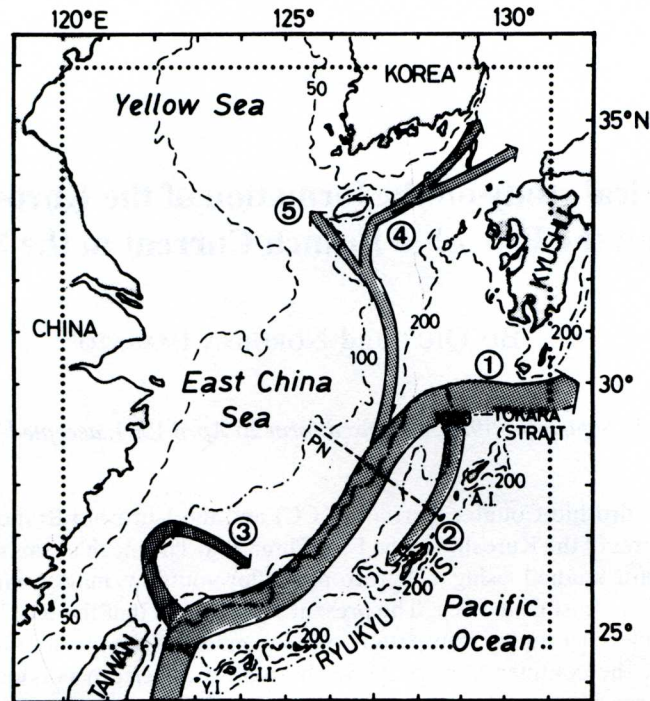


Fig. 1. Schematic flow pattern of the Kuroshio in the East China Sea: (1) the Kuroshio main stream; (2) the Kuroshio Counter Current (KCC); (3) the Kuroshio Branch Current (KBC); (4) the Tsushima Warm Current and (5) the Yellow Sea Warm Current. The depth contour of the bottom topography is in meters. Y.I., I.I. and A.I. indicate the islands of Yonakuni-jima, Ishigaki-jima and Amami-oshima, respectively. The dashed-line PN shows the stationary observational section by Nagasaki Marine Observatory.

autumn (19.78 Sv), as compared with its annual mean value of 22.67 Sv (FUJIWARA, 1981). Based on GEK data observed along the PN section from 1956 to 1975, GUAN and MAO (1982) also confirmed the existence of the KCC. They estimated the maximum speed of the KCC to be 20 cm s^{-1} on average. A more detailed long-term averaged surface velocity pattern for the entire East China Sea is shown in Fig. 3, wherein we averaged the GEK data compiled by the Japan Oceanographic Data Center for the period of 1953–1984 at each mesh area of $12' \times 12'$. The result of Fig. 3 reveals that the KCC is not a flow confined near the PN section, but rather exists throughout the offshore areas from Amami-oshima Island to Ishigaki-jima Island between the Kuroshio and the Ryukyu Islands.

Another noteworthy feature of the Kuroshio in the East China Sea is that a branch current separating from the Kuroshio forms immediately after the Kuroshio passes by the east coast of Taiwan (see Fig. 1). The existence of this branch current (the Kuroshio Branch Current, KBC) is verified by the averaged flow pattern of Fig. 3. Figure 3 shows that the KBC has a tendency to turn to east-southeast to rejoin the main stream of the Kuroshio after it flows onto the continental shelf north of Taiwan. The KBC's presence on the shelf north of Taiwan is also confirmed by recent satellite pictures. One such picture taken by the NOAA-8 satellite on 3 January 1984 is shown in Fig. 4. The dark tones in the picture represent warm Kuroshio water and the light tones represent cold shelf-originated waters. From Fig. 4, it is clear that a dark-toned water mass extends over the continental shelf north of Taiwan, suggesting that a part of the Kuroshio has been transported onto the

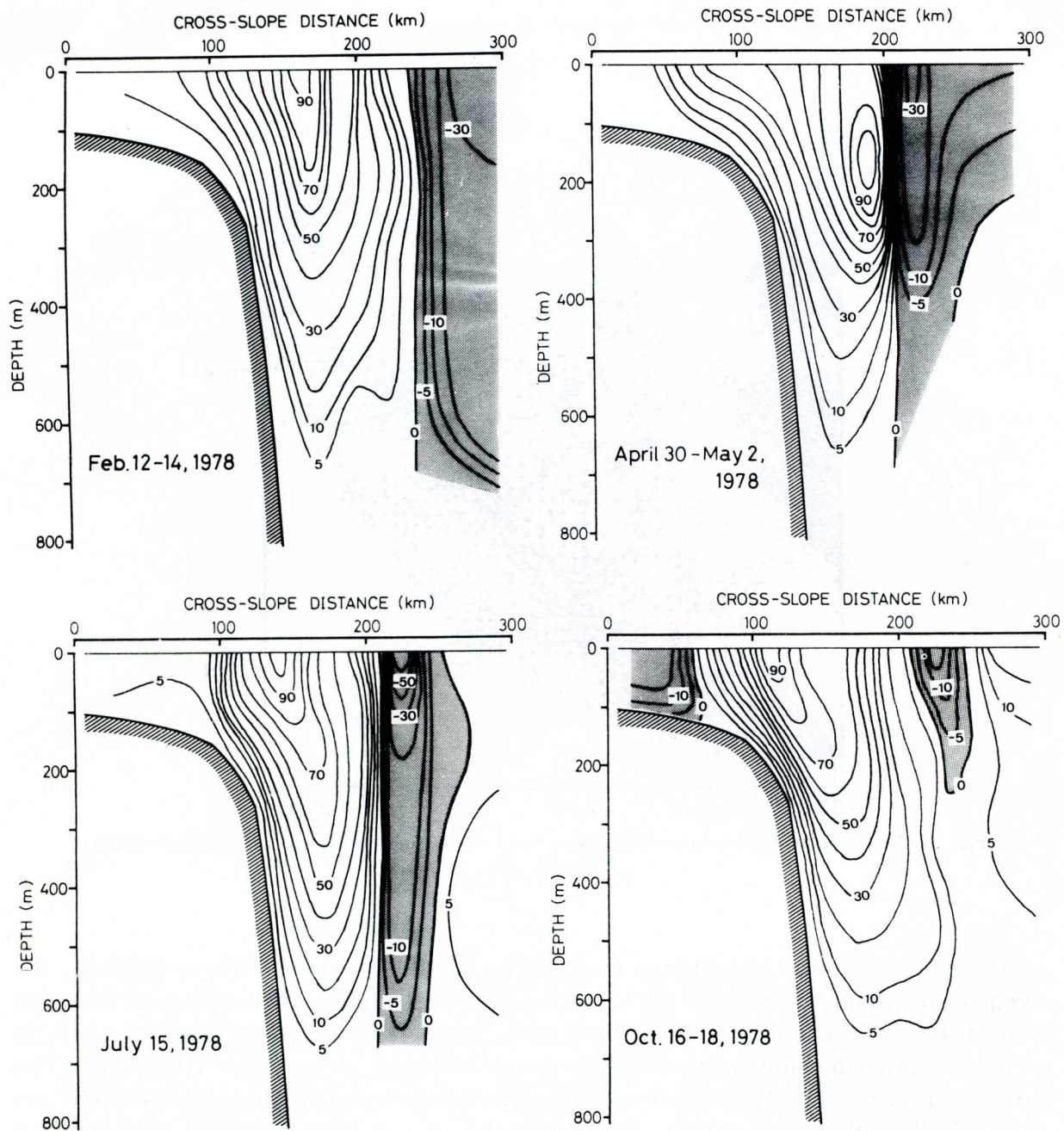


Fig. 2. Geostrophic velocity profiles along the PN section in four different seasons in 1978 (after INOUE, 1981). The unit for velocity contours is in cm s^{-1} and the offshore hatched regions indicate the KCC.

shelf by the KBC. According to INOUE (1981), the warm water mass of the KBC can sometimes reach the mouth of Yangtze River.

In addition to the KCC and the KBC, the Tsushima Warm Current is another important branch of the Kuroshio in the East China Sea. Evidence that the Tsushima Warm Current separates from the Kuroshio was presented by HUH (1982a,b). MINATO and KIMURA (1980) claimed that the generation mechanism of the Tsushima Warm Current is a result of the pressure difference between the East China Sea and the Tsugaru Strait. On the other hand, ICHIYE (1984) proposed that the residual lateral transport of the Kuroshio through the Reynolds' stresses causes the Tsushima Warm Current.

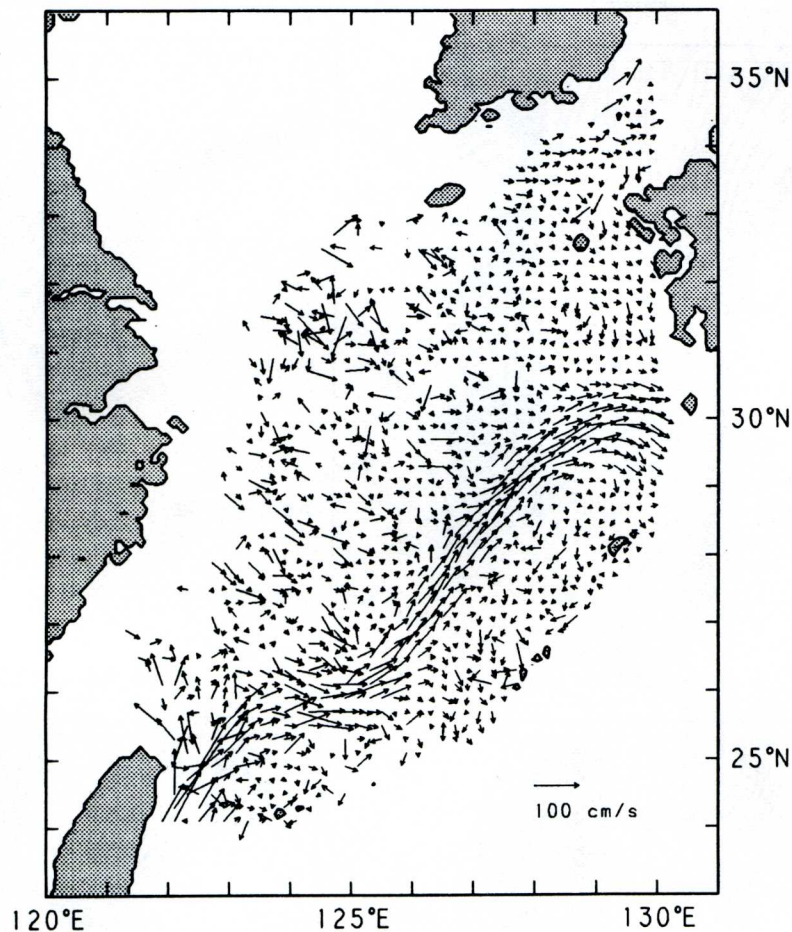


Fig. 3. Surface flow pattern in the East China Sea derived from the long-term GEK observations (1953–1984).

Compared with the generation mechanism of the Tsushima Warm Current, the mechanisms which generate the KCC and the KBC are still unknown. Although the main body of the Kurishio does not flow directly over the shallow continental shelf, the KBC in particular, crucially influences the water mass exchange in the East China Sea. The purpose of the present study is to understand the mechanisms that generate the KCC and the KBC. In our first approach, we adopt a barotropic inflow–outflow model with a simplified coast configuration and bottom topography of the East China Sea. The importance of external physical factors on the KCC and the KBC, such as the planetary β -effect and the presence of Taiwan and the Ryukyu Islands, is investigated.

2. MODEL DESCRIPTION

A schematic view of the model basin is shown in Fig. 5. The basin has two openings both 80 km in width located in the outer ocean. The inflow opening at the southern wall corresponds to the strait between Taiwan and Yonakuni-jima Island, and the outflow opening at the east wall corresponds to the Tokara Strait. The existence of the Tsushima Strait is not considered in the present study because we expect its influence on the formation of the KCC and the KBC to be insignificant. A slope running northeast–

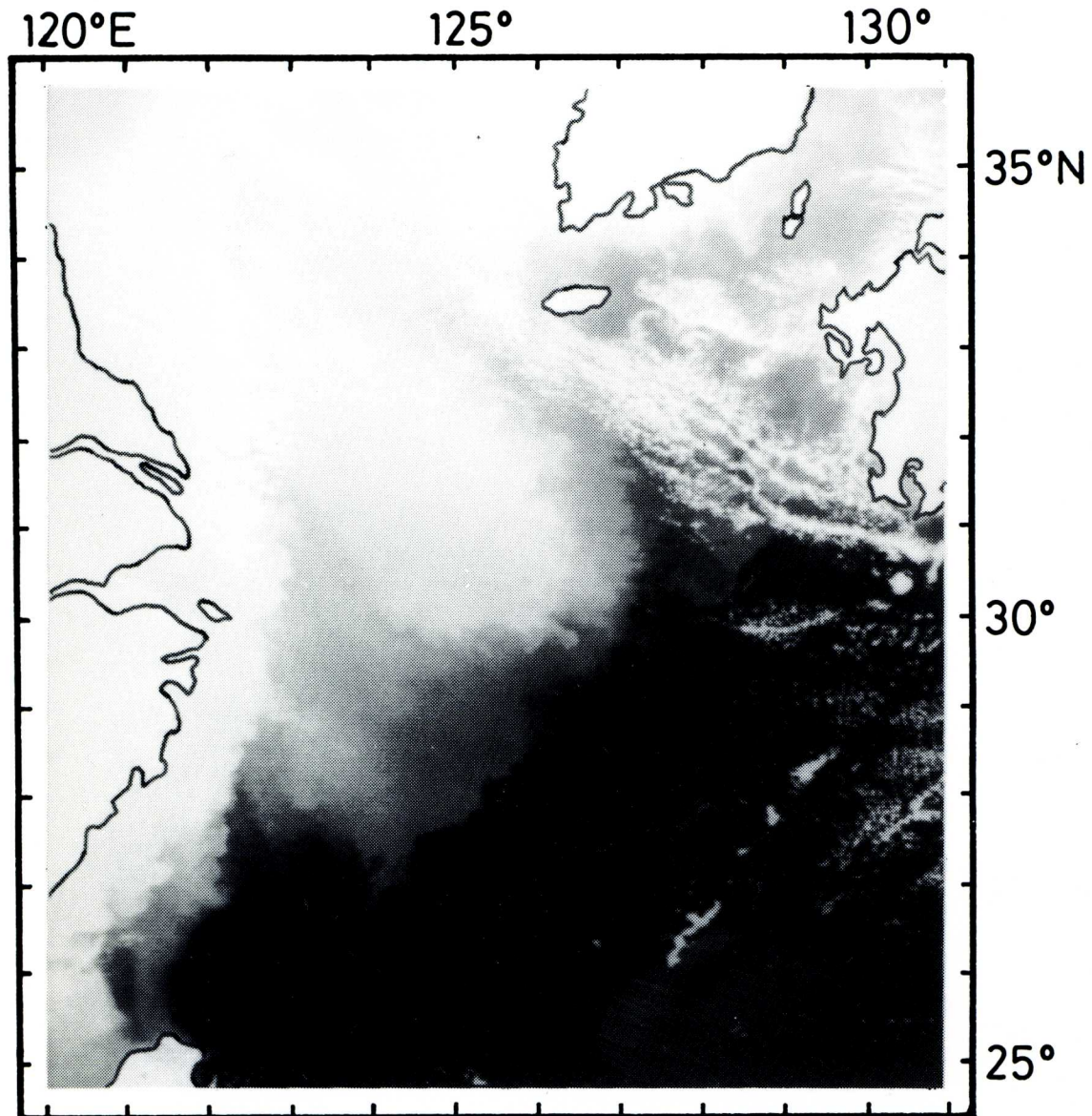


Fig. 4. Thermal infra-red picture of the surface temperatures in the East China Sea taken by the NOAA-8 satellite on 13 January 1984. The picture's area is also outlined by the dotted line in Fig. 1. Darker tones represent Kuroshio water at a higher temperature.

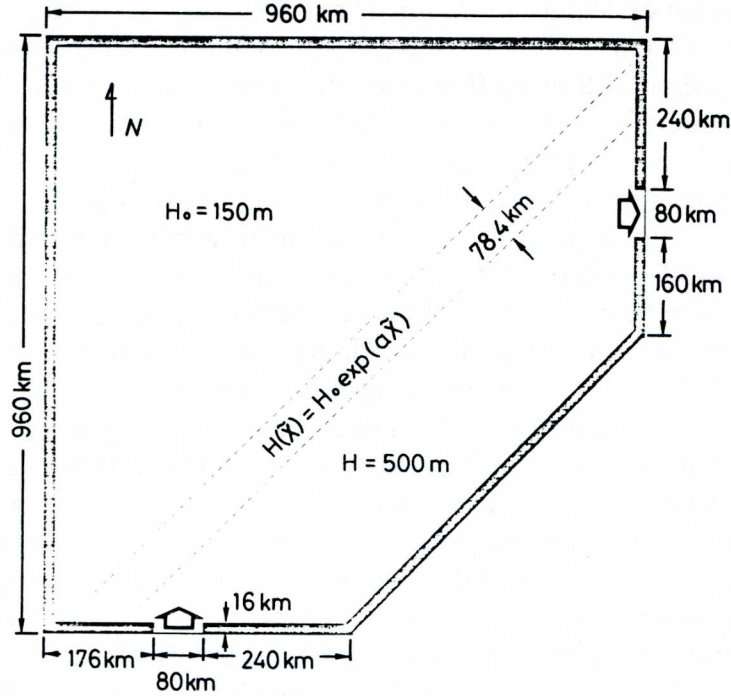


Fig. 5. Basin configuration and bottom topography used as the basic inflow–outflow model. A continental slope of the exponential form ($\alpha = 0.0152 \text{ km}^{-1}$) is located between the broken lines. Both the continental shelf and the outer ocean have flat bottoms.

southwest in the model basin (indicated by broken lines in Fig. 5) represents the continental slope in the East China Sea. It has a simple form of $H(\bar{X}) = H_0 \exp(\alpha \bar{X})$, where \bar{X} is the offshore distance from the shelf break and α is 0.0152 km^{-1} , an average slope inclination in the East China Sea. Although the depth of the outer ocean beyond the continental slope is actually about 1000 m, we set the depth at 500 m for this study because the main body of the Kuroshio flows only above this top layer (see Fig. 2). The shallow continental shelf has a uniform depth of $H_0 = 150 \text{ m}$. A wall parallel to the continental slope located southeast of the outer ocean represents the Ryukyu Islands.

The basin configurations of Fig. 5 are a high simplification of those in Fig. 1, because we are mainly concerned with the dynamics of the formation of the KCC and the KBC rather than simulating realistic flow patterns. The size of the model basin ($960 \times 960 \text{ km}$) is, however, about the same as that of the East China Sea. Three modified basin configurations in which the Ryukyu Islands or Taiwan Island are absent are also adopted in order to investigate the topographical effects. These modifications will be discussed later.

The model's governing equation is the barotropic potential vorticity equation under the approximations of rigid-lid and β -plane:

$$\zeta_t + (-h^{-1}\phi_y \zeta)_x + (h^{-1}\phi_x \zeta)_y + \beta h^{-1}\phi_x - f_o h^{-2} J(\phi, h) = A_h \nabla^2 \zeta, \quad (1)$$

where subscripts (x, y, t) denote partial differentiation; ϕ is the volume transport stream function; $h(x, y)$ is the basin depth; ∇_h^2 is the horizontal Laplacian operator; J is the Jacobian operator; and ζ is the vertical component of the relative vorticity, which is related to ϕ by $\zeta \equiv (h^{-1}\phi_x)_x + (h^{-1}\phi_y)_y$. In this study, we express sub-grid-scale mixing processes in the form of horizontal eddy diffusion, which has a coefficient of $A_h = 10^7 \text{ cm}^2 \text{ s}^{-1}$. This specific value of A_h is chosen so that the jet width corresponds to that of the observed

Kuroshio (see Section 4). Values for f_o and β are $6.15 \times 10^{-5} \text{ s}^{-1}$ (referred at 20°N latitude) and $2.0 \times 10^{-13} \text{ s}^{-1} \text{ cm}^{-1}$, respectively. Inflow volume transport from the southern opening is set at either 28.8 or 18.0 Sv, the representative values in the large and small inflow seasons, respectively (FUJIWARA, 1981). The same amount of volume flows out through the east opening to ensure mass conservation.

The initial condition of the model is that a strong jet exists in the middle of the outer ocean. Calculations with the initial jet at various locations reveal that the final quasi-steady flow patterns do not depend on the jet's initial location. As for the boundary conditions, we fix the stream function ϕ at the inflow and outflow openings, such that the jet has a triangle velocity profile. We also did calculations with a self-determined outflow condition, that is, $\partial\phi/\partial x = 0$ and $\partial^2\phi/\partial x\partial y = 0$ at the outflow opening. The results showed that this condition would alter the flow pattern near the outflow opening, but not the patterns of the counter current and the branch current. Since the present study is mainly concerned with the KBC and the KCC, the fixed outflow condition, which requires less computational time to reach the quasi-steady state, is adopted in the following calculations. A slip condition, $\partial^2\phi/\partial n^2 = 0$, is applied at the rigid walls, where n directs perpendicularly to the walls. The slip boundary condition is used because the walls in the model basin do not necessarily correspond to the realistic coast lines. Calculations with the no-slip boundary condition show that the patterns of the KBC and the KCC are exactly the same regardless of the type of wall condition.

Equation (1) is numerically integrated until the motion in the model basin reaches its quasi-steady state. The horizontal grid-sizes used in the numerical calculations are 16 km in both directions. This grid-size value is small enough to resolve both the KBC and the KCC, whose typical length scales are of $O(40 \text{ km})$ and $O(150 \text{ km})$, respectively.

3. NUMERICAL RESULTS

Figure 6 shows the quasi-steady flow pattern of Case 1 obtained when the β -effect is neglected in the model basin. The inflow volume transport is 28.8 Sv (see Table 1 for the difference in the inflow volume transport and other external parameters used in the different model cases). From Fig. 6 we notice that the inflow jet deflects offshoreward and its width widens after it hits the continental slope. Although a return flow is induced in the southeastern corner of the basin, it cannot be regarded as a counter current of the same magnitude as the KCC. This is because the KCC, as we noticed in Fig. 3, occupies the entire region between the Kuroshio and the Ryukyu Islands, while in Case 1, no southwesterly flows are present near the outflow opening (the Tokara Strait). From Fig. 6 we also notice that only a small part of the inflow jet near the inflow opening crawled onto the continental slope. Over the southwest shelf, a cyclonic circulation is induced due to the viscosity. This circulation moves in the opposite direction to that of the KBC. Consequently, on the f -plane frame of reference, neither the KCC nor the KBC can be generated.

When the β -effect is included (Case 2), Fig. 7 shows that the inflow jet is pushed strongly against the continental slope and has the same width of about 150 km throughout the basin area. Moreover, a counter current is induced offshore over the whole outer ocean region along the southeast wall. The facts that the calculated jet width remains the same at about 150 km and that the counter current extends over the entire offshore region, agree well with the observational results of Fig. 3. In Fig. 7 it is also clear that a part of the inflow jet

branches onto the continental shelf along the southern wall left of the inflow opening. This branch current moves anticyclonically over the shelf and eventually returns back to the main stream over the continental slope. Although the calculated branch current is large in scale, it resembles the observed branch current pattern shown in Fig. 3 (a more detailed calculation of the branch current will be given in Case 6, Fig. 11).

The same flow pattern as in Case 2 is obtained in Case 3 (Fig. 8), wherein we reduced the inflow volume transport from 28.8 to 18.0 Sv, corresponding to the Kuroshio in autumn. In Case 3, a reduction from 5.5 to 3.8 Sv occurred in the volume transport of the counter current. This result agrees qualitatively with the seasonal changes of the KCC as observed in Fig. 2. Although the influence of the inflow transport of the Kuroshio on the KBC is unknown due to a scarcity of observation data, the numerical results of Figs 7 and 8 suggest that the KBC would also weaken if the Kuroshio's transport decreases.

In order to investigate the influence of the Ryukyu Islands on the formation of the KCC, we calculated two more cases (Cases 4 and 5) that are similar to Cases 1 and 2 except for the absence of the southeast wall in the outer ocean. The flow patterns together with the basin configuration are shown in Figs 9 and 10. Comparing the offshore flow pattern in Fig. 9 with that in Fig. 6 reveals that the scale and magnitude of the return flow in the f -plane cases are essentially controlled by the southeast wall. The inclusion of a realistic southeast wall (i.e. the Ryukyu Islands) may confine the return flow to about 20 cm s^{-1} , similar to the magnitude of the KCC. But as discussed above, this southeast wall is not the determinant condition in the formation of the KCC.

On the contrary, Fig. 10 shows that after including the β -effect, a counter current similar

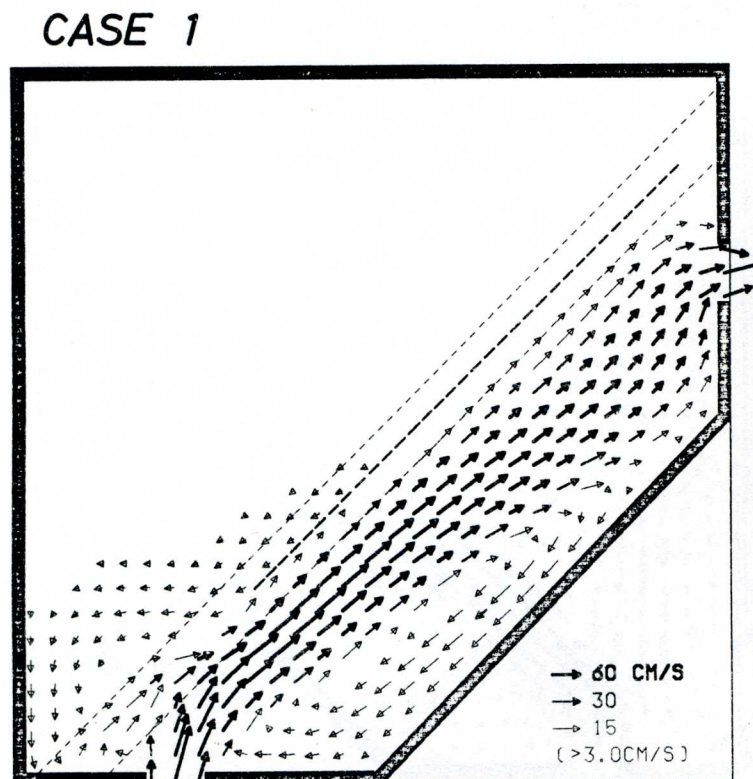


Fig. 6. Quasi-steady flow pattern of Case 1, in which the inflow volume transport is 28.8 Sv and the planetary β -effect is excluded. The model basin is that of Fig. 5.

Table 1. External parameters used in the different numerical calculations

Case no.	β -effect	Inflow volume transport (Sv)	Southeast wall	Slope on the shelf
1	<i>x</i>	28.8	<i>o</i>	<i>x</i>
2	<i>o</i>	28.8	<i>o</i>	<i>x</i>
3	<i>o</i>	18.0	<i>o</i>	<i>x</i>
4	<i>x</i>	28.8	<i>x</i>	<i>x</i>
5	<i>o</i>	28.8	<i>x</i>	<i>x</i>
6	<i>o</i>	28.8	<i>o</i>	<i>o</i>

to that obtained in Fig. 7 can exist even without the existence of the Ryukyu Islands. The volume transport of the counter current in Fig. 10 shows a larger value (7.8 Sv) than in Fig. 7 (5.5 Sv) due to an anticyclonic circulation induced in the further outer ocean. The results of Figs 7 and 10 thus suggest that, while the existence of the Ryukyu Islands may quantitatively affect details of the KCC, it is the β -effect that is essential in generating it. The role played by the β -effect will be considered again in the next section.

In Figs 7 and 8, the calculated branch current over the continental shelf reached the west wall of the basin. However, both the surface flow pattern of Fig. 3 and the satellite picture of Fig. 4 showed that the real KBC is more or less confined in the northern sea area of

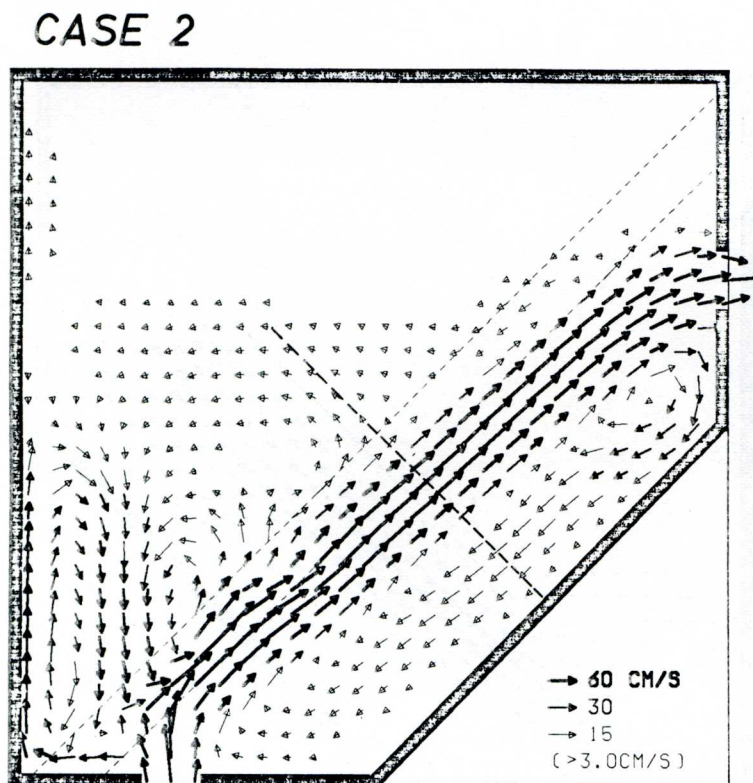


Fig. 7. Quasi-steady flow pattern of Case 2. The external parameters are the same as in Case 1 except for the inclusion of the β -effect.

CASE 3

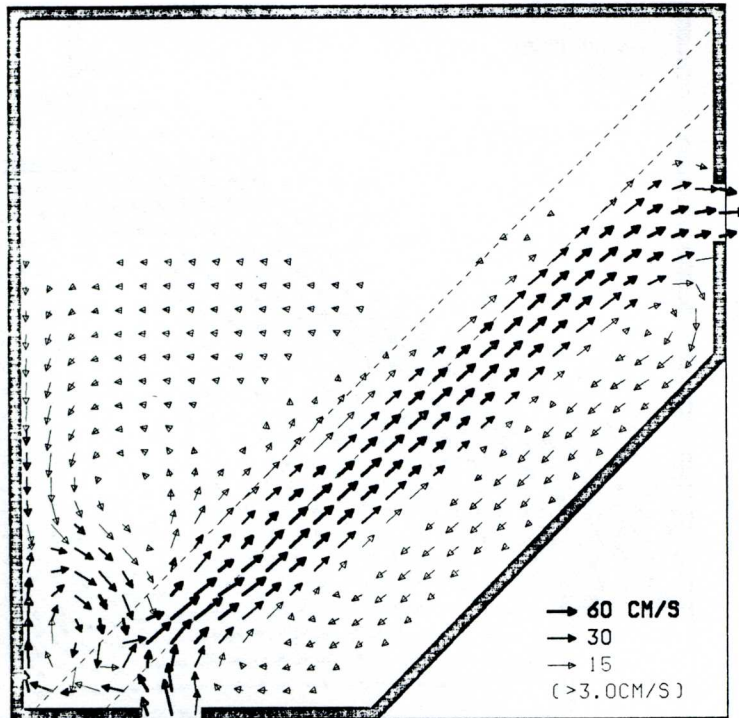


Fig. 8. Quasi-steady flow pattern of Case 3. The external parameters are the same as in Case 2 except that the inflow volume is reduced to 18.0 Sv, corresponding to the inflow of the Kuroshio in autumn.

Taiwan. This discrepancy can easily be resolved if we include a more realistic topography with a gentle bottom inclination over the continental shelf. Figure 11 shows the numerical result in Case 6 when a shallow layer of 100 m is added over the continental shelf. Also included in Case 6 is the projection of Taiwan Island, which renders the basin configuration near the inflow opening closer to the real topography (Fig. 1). Compared with Case 2, the result of Case 6 shows that the motion over the 100 m shelf is largely suppressed and that the main body of the branch current returns back to the Kuroshio main stream without reaching the western wall. Both features are a better realization of the observed KBC pattern (Fig. 3).

4. DISCUSSIONS

In the last section, we calculated the quasi-steady motions in a barotropic inflow-outflow model and obtained flow patterns similar to the KCC and the KBC observed in the East China Sea. Based on these numerical results, further investigations into the generation mechanisms of the KBC and the KCC will be discussed in this section.

4.1. Factors that determine the pattern of the KCC

In the light of Munk's boundary layer theory, it is not surprising that an offshore counter current exists next to a western boundary current. By balancing the planetary vorticity acquisition of the northward-flowing current with the lateral diffusion of the relative

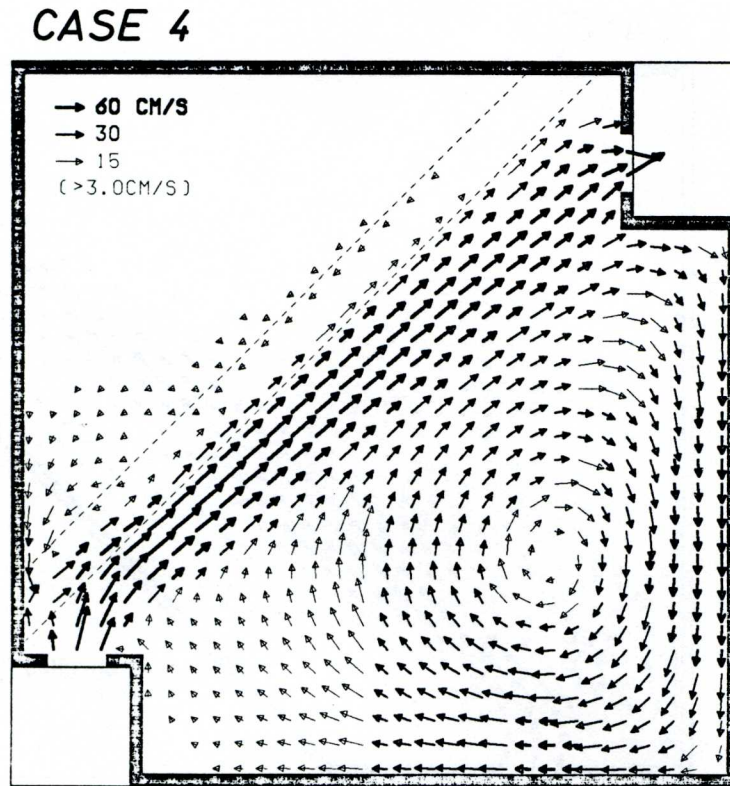


Fig. 9. Quasi-steady flow pattern of Case 4 on the f -plane of reference. In this case, the offshore wall (the Ryukyu Islands) is removed, while the other basin conditions are kept the same as in Fig. 5.

vorticity, Munk's theory predicts that a counter current with a width of $2\pi (A_h/\beta)^{1/3}/\sqrt{3}$ should appear in the offshore side of the boundary current (e.g. PEDLOSKY, 1979).

In Fig. 12, we calculated the velocity profiles and the vorticity balance along a cross-slope line in Case 2 (see Fig. 7 for the line's location). In Fig. 12a, the velocity components perpendicular and parallel to the continental slope are u and v , respectively. Notice that the cross-slope component of the velocity u is not zero, due to offshoreward deflection of the boundary current from the continental slope. In the vorticity balance of Fig. 12b, this velocity component renders the vortex stretching term $f_\delta h^{-2} J(\phi, h)$ to be dominant over the continental slope. In Munk's boundary layer theory, the western boundary is assumed to be a vertical wall and the eastern boundary far away. Given the Kuroshio in the East China Sea, it is, however, important to further understand whether a sloping western boundary, a cross-slope deflection of the boundary current, as well as a close "eastern" wall (the Ryukyu Islands) can affect the pattern of the KCC. These questions are investigated below.

First, we fix the coordinates (\tilde{X}, \tilde{Y}) on the topography and the coordinates (X, Y) on the boundary current, such that the \tilde{Y} -axis is along the slope and the Y -axis is parallel to the boundary current (see Fig. 13). If the angle between the \tilde{Y} - and Y -axis is η , the slope, $H(\tilde{X}) = H_1 \exp(\alpha \tilde{X})$, can then be expressed in the (X, Y) -coordinates as

$$H(X, Y) = H_1 \exp [\alpha (X \cos \eta + Y \sin \eta)]. \quad (2)$$

Suppose the motion is steady and its variation in the along-stream direction is slower than

that in the cross-stream direction. The vorticity equation (1) at the lowest order in the (X, Y) -coordinates then reduces to

$$\beta \cos(\theta + \eta)V - f_o H^{-1} H_Y V = A_h V_{XXX}, \quad (3)$$

where $V(X)$ is the along-stream velocity, and θ is the angle between the \tilde{Y} -axis and the north direction, which is 45° in the present model (see Fig. 5). Substituting (2) into (3) yields

$$[\beta \cos(\theta + \eta) - f_o \alpha \sin \eta]V = A_h V_{XXX}, \quad (4)$$

which is again the Munk's balance except that the effective β value in equation (4) includes the topographic effect. Assuming the current is western-intensified, we obtain the following solution to equation (4):

$$V(X) = \begin{cases} \exp(-K'X/2)[C_1 \cos(\sqrt{3K'X}/2) + C_2 \sin(\sqrt{3K'X}/2)] & (-L \leq X < 0) \\ \exp(-KX/2)[C_3 \cos(\sqrt{3KX}/2) + C_4 \sin(\sqrt{3KX}/2)] & (0 < X \leq W), \end{cases} \quad (5)$$

where $K' \equiv [\{\beta \cos(\theta + \eta) - f_o \alpha \sin \eta\}/A_h]^{1/3}$, $K \equiv [\alpha \cos(\theta + \eta)/A_h]^{1/3}$, L is the distance over the slope onto which the boundary current intrudes, and W is the offshore distance of the eastern wall. In solution (5), C_i ($i = 1-4$) are constant values determined by the following conditions:

CASE 5

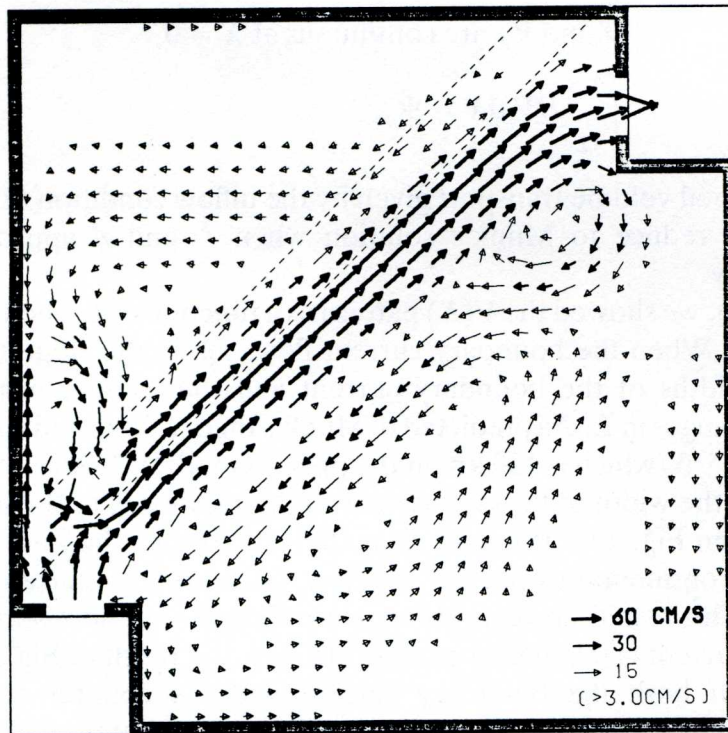


Fig. 10. Quasi-steady flow pattern of Case 5. The external parameters are the same as in Case 4 except on the β -plane of reference.

CASE 6

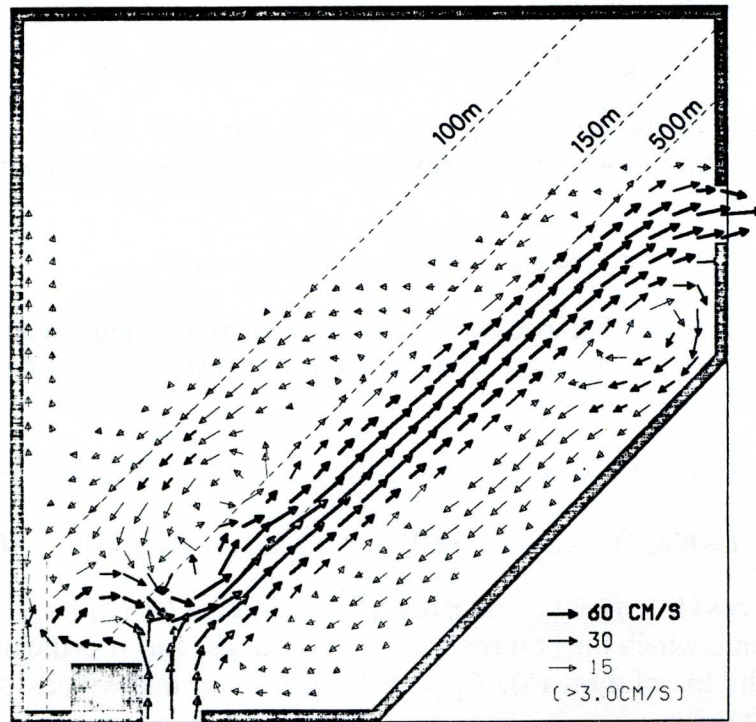


Fig. 11. Quasi-steady flow pattern of Case 6. The model basin is similar to Fig. 5 with the addition of a shallow layer of 100 m and the projection of Taiwan Island over the continental shelf.

$$V = 0 \text{ at } X = -L,$$

$$V \text{ and } V_X \text{ are continuous at } X = 0, \quad (6)$$

$$\int_{-L}^W HV \, dX = \Psi_o,$$

where, Ψ_o is the total volume transport given by the inflow condition (28.8 Sv). Note that equations (4)–(6) reduce to Munk's solution when L and η approach zero and W approaches infinity.

In Fig. 14a and b, we showed the $V(X)$ pattern as a function of L when η is set to be 0 and 1.5° , respectively. When the boundary current flows along the slope ($\eta = 0^\circ$), Fig. 14a shows that the widths of the boundary current and the counter current offshore are independent of changes in L . As predicted in Munk's theory, both widths are given by $M = 2\pi (A_h/\beta \cos \theta)^{1/3}/\sqrt{3}$ (which is 150 km in the present model). Notice that when $L + W$ is smaller than $2M$, the width of the counter current narrows due to the interception of the offshore wall. From Fig. 14a, it is also clear that the further the boundary current may intrude onto the continental slope, the stronger the boundary current and the counter current become. This result, however, is negated when the offshoreward deflection effect of the boundary current is taken into account. In fact, the result of Fig. 14b indicates that the magnitudes of both the boundary current and the counter current are mostly independent of the L changes. In Fig. 14b, we further notice that the width of the boundary current varies with the change in L : a larger L leads to a wider current width. This tendency also appears in the numerical result of Case 2 (Fig. 7). The width of the counter current, on

the other hand, is not influenced by the L changes, except that the offshore wall interception can again narrow the flow width. From the results of Fig. 14, we conclude that due to the offshoreward deflection of the boundary current in the slope region, the presence of the sloping western boundary does not significantly influence the pattern of the counter current.

In Fig. 15, we calculated the $V(X)$ patterns when $L = 52$ km, $\eta = 1.5^\circ$ and W is parametrically changed. The result of Fig. 15 clearly shows that when $W > 250$ km, the patterns of the boundary current and the counter current become insensitive to the W values. Since W in the East China Sea is 250 km on average, we conclude that the existence of the Ryukyu Islands also has an insignificant influence on the pattern of the KCC. This conclusion is consistent with the numerical results of Cases 2 and 5.

4.2. Mechanisms that cause the KBC

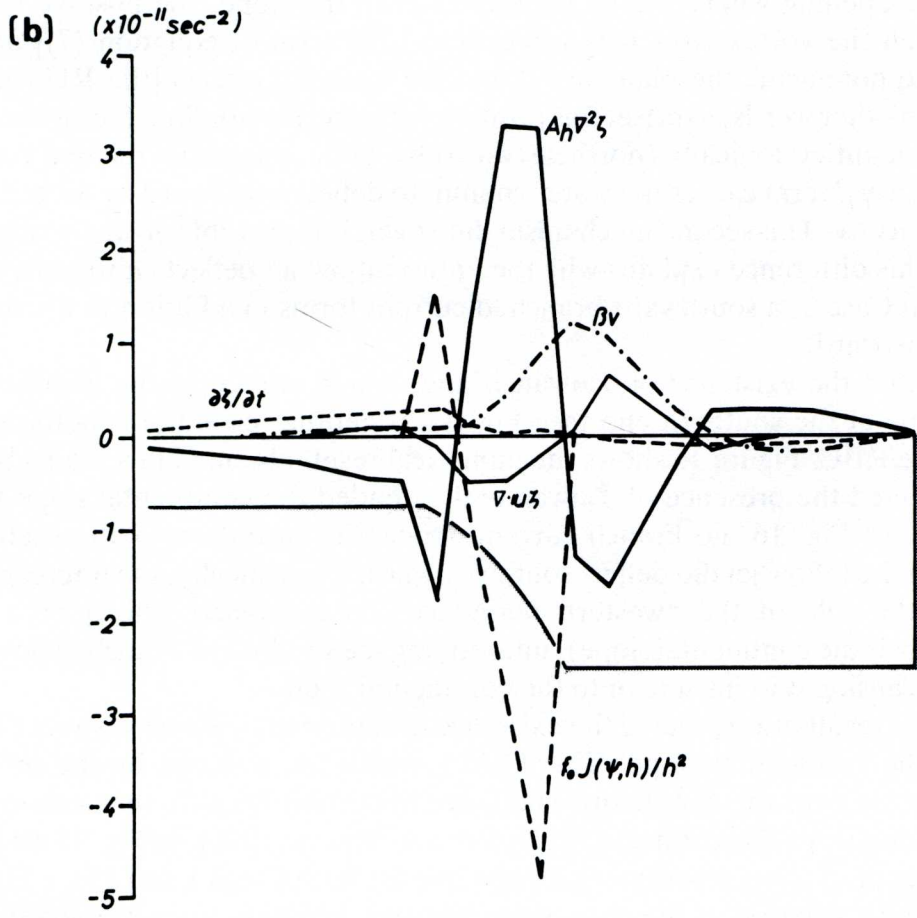
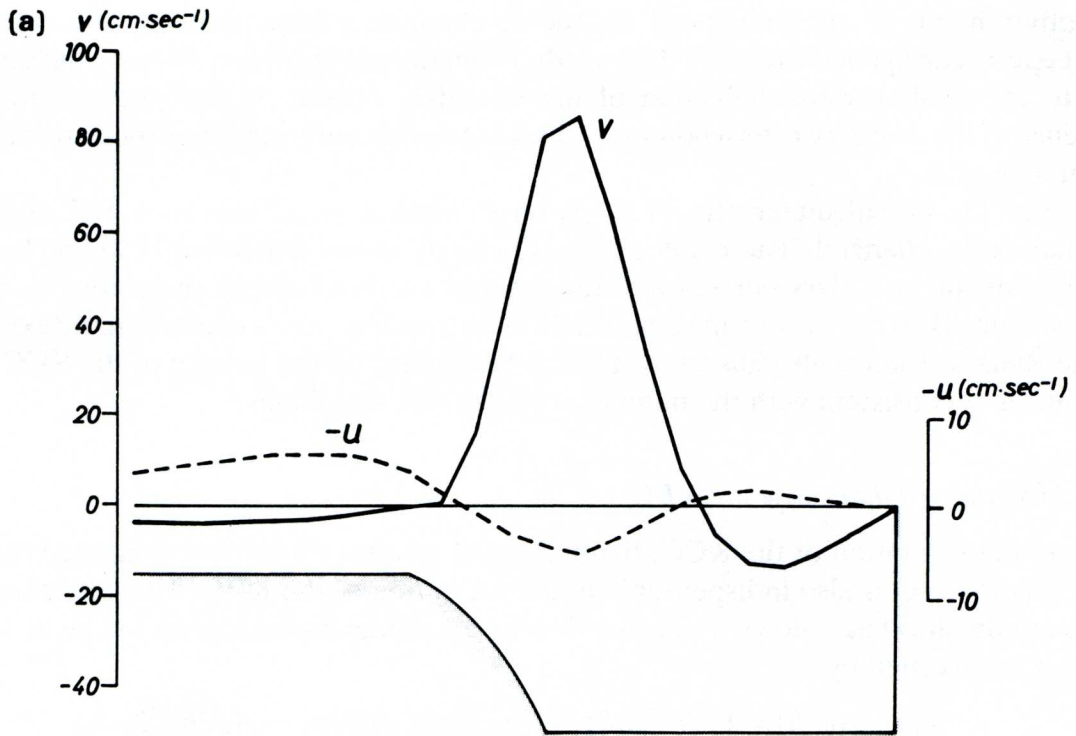
As in the formation of the KCC, the numerical results in Section 3 suggested that the planetary β -effect is also indispensable in the formation of the KBC. This β dependency can be understood as follows. After the flow in the model basin reaches the quasi-steady state, it is governed by

$$f_o h^{-2} J(\phi, h) = (-h^{-1} \phi_y \zeta)_y + (h^{-1} \phi_x \zeta)_y \beta h^{-1} \phi_x - A_h \nabla h^{-2} \zeta. \quad (7)$$

Near the inflow opening where the jet penetrates onto the slope, the positive vorticity acquired through the vortex stretching effect [the LHS term of equation (7)] must be balanced by the nonlinear, the planetary β and the viscosity effects [the RHS term of equation (7)]. In other words, to offset this positive vorticity, the nonlinear term causes the inflow jet to turn anticyclonically (northeastward) by gaining negative relative vorticity, while the planetary β term causes the water column to deflect southward by decreasing its planetary vorticity βy . This second mechanism, however, is impossible on an f -plane frame of reference. This difference explains why the entire inflow jet deflects northeastward in Case 1, while in Case 2, a southward-branched current forms in addition to the main jet flowing northeastward.

Also notice that the existence of Taiwan Island, which intercepts the isobars of the continental slope at the southern end (see Fig. 1), is another essential condition in the formation of the KBC. Figure 16 shows the numerical result obtained in a model basin in which we neglected the presence of Taiwan and extended the continental slope further southwestward. In Fig. 16, no branch current appears to intrude over the shelf, even though a part of the inflow jet did deflect southwestward. Dynamically, the interception of Taiwan plays the role of the “western boundary” on a β -plane (the β here is the topographic β over the continental slope), intensifying the southward-branched flow north of Taiwan and causing it to intrude onto the continental shelf.

The numerical result also revealed the existence of topographic Rossby waves (TRWs) trapped near the continental slope. The TRWs, which are induced by the inflow jet repeatedly crossing over the continental shelf, are important because they convey wave energy in the along-slope direction (e.g. LEBLOND and MYSAK, 1978). In Fig. 17 we plotted the time changes of u' along a continental slope line for both Cases 1 and 2 (see Fig. 6 for the line's location), where u' is the cross-slope velocity deviation from its time-averaged value. From the inclination of the u' contours, we find that the waves in both cases have a phase propagation in the negative \tilde{Y} -direction (i.e. moving southwestward). The wave



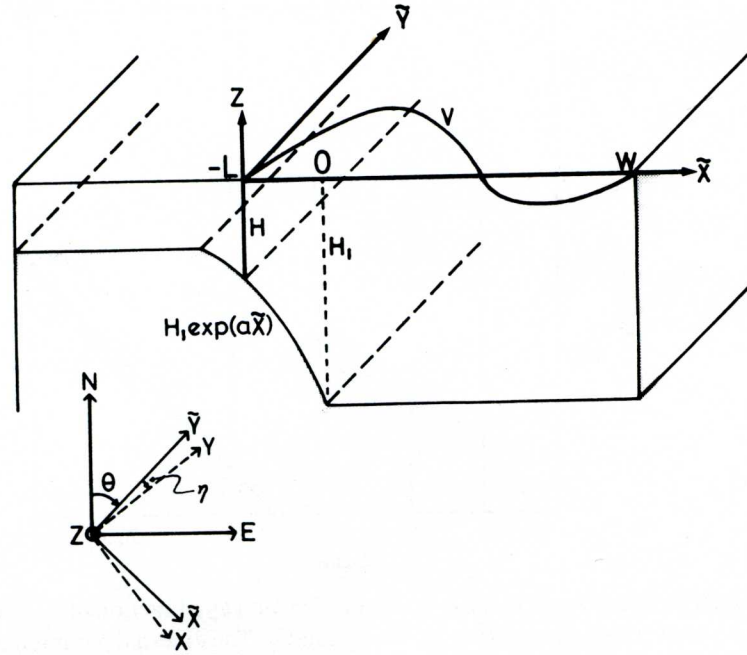


Fig. 13. The (\bar{X}, \bar{Y}) and (X, Y) coordinate systems. L is the width over the slope onto which the boundary current penetrates and W is the distance of the offshore wall from the slope edge.

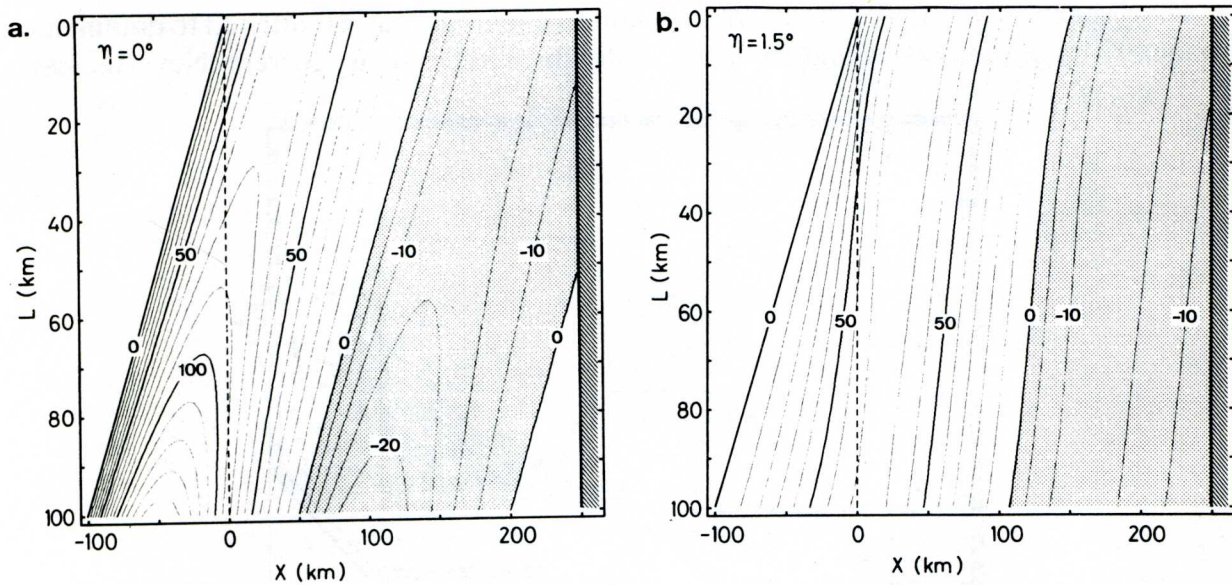


Fig. 14. Analytical flow pattern in the cross-slope direction as a function of L , the width over the slope onto which the boundary current penetrates. In (a), $\eta = 0^\circ$: no cross-slope effect of the boundary current is considered. In (b), $\eta = 1.5^\circ$: a typical deflection angle obtained in the numerical result of Case 2. In the figures, contour values are in cm s^{-1} and the external parameters are given by $H_1 = 500 \text{ m}$, $\alpha = 0.0152 \text{ km}^{-1}$, $\Psi_0 = 28.8 \text{ Sv}$ and $W = 250 \text{ km}$.

Fig. 12. (a) Velocity profiles obtained in Case 2 along a cross-slope line (its location is indicated by the broken line in Fig. 7), where u and v are the velocity components perpendicular and parallel to the slope, respectively. (b) Term balances in the vorticity equation along the same cross-slope line as in (a). Names of each term correspond to those defined in equation (1).

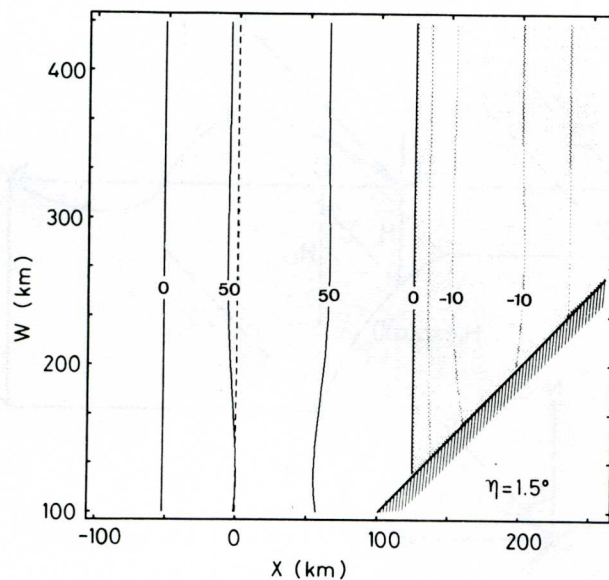


Fig. 15. Analytical flow pattern in the cross-slope direction as a function of W , the width between the slope edge and the offshore wall (the Ryukyu Islands). The external parameters are those used in Fig. 14 with $L = 52$ km.

length and the wave period in Case 1 are 360 km and 3.2 days (Fig. 17a), while in Case 2 they are 624 km and 2.4 days (Fig. 17b).

The dispersion relation of the TRWs relevant to our model basin is difficult to obtain due to the existence of viscosity and the horizontally sheared boundary current. Nevertheless,

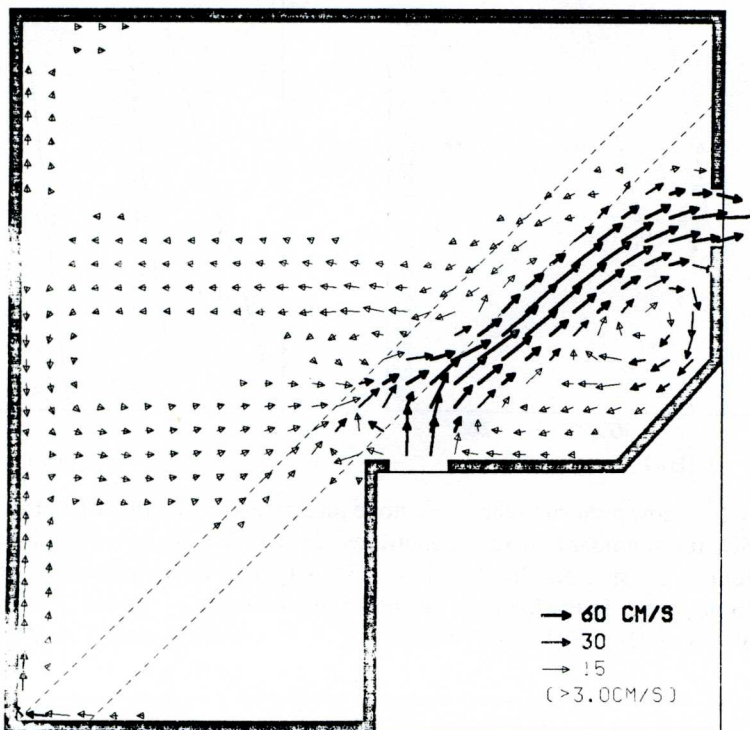


Fig. 16. Quasi-steady flow pattern in the model basin wherein Taiwan Island is neglected and the continental slope is extended further southwestward. The model has an inflow volume transport of 28.8 Sv and is on the β -plane of reference.

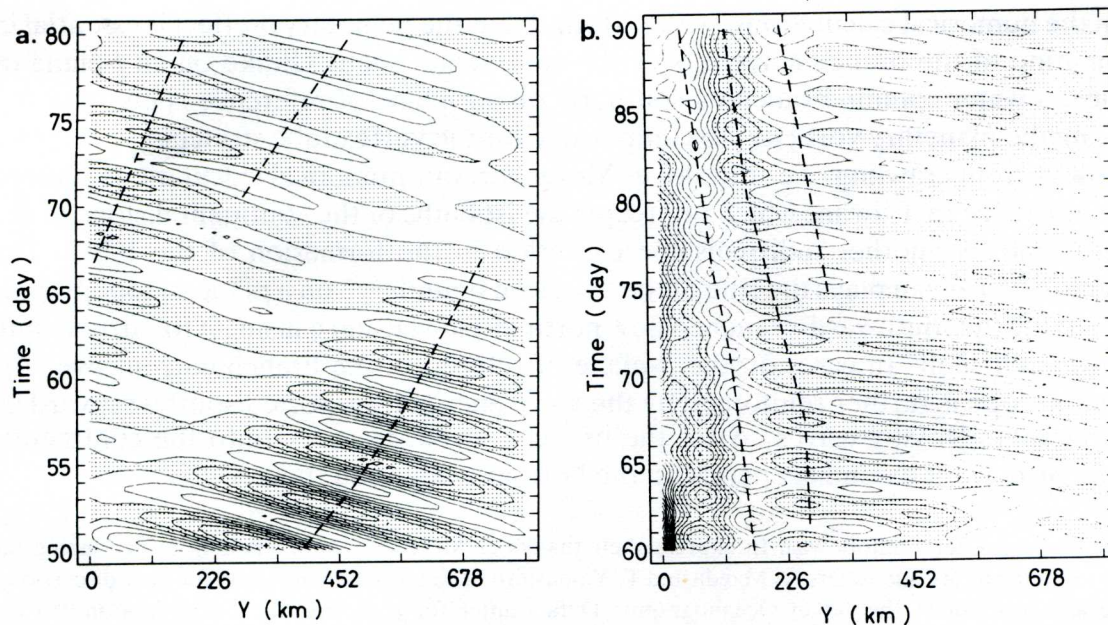


Fig. 17. Temporal variations of u' along the continental slope as shown by the dashed line in Fig. 6, where u' is the cross-slope velocity deviation from its time-averaged value. (a) gives the result on the f -plane (Case 1) and (b), on the β -plane (Case 2). The contour values are 0.05 cm s^{-1} for (a) and 0.10 cm s^{-1} for (b). The shaded regions indicate negative values.

judging from the propagation of the wave envelopes in Fig. 17, we find that the group velocity of the TRWs in Case 1 is in the positive \tilde{Y} -direction (as indicated by the broken lines), while in Case 2 it is in the negative \tilde{Y} -direction. Since the wave energy moves with the group velocity, results of Fig. 17 suggest that the TRWs convey the wave energy southwestward in the β -plane case. This energy conveyance by the TRWs consequently reinforces the branch current at the southwestern end of the slope.

5. CONCLUSIONS

Using a barotropic inflow–outflow model with a simplified coast configuration and bottom topography of the East China Sea, we studied the mechanisms that cause the KCC and the KBC, two major features of the Kuroshio in the East China Sea.

From the numerical calculations, we found that the counter current parallel to the Kuroshio can only exist on the β -plane frame of reference. The mechanism supporting this counter current is the balance between the planetary vorticity acquired by the Kuroshio as it flows northwards and the lateral diffusion of the relative vorticity (that is, the Munk's balance). The offshore Ryukyu Islands are found to exert little influence on the pattern and magnitude of this counter current. From the numerical results, we also found that the maximum velocities of the counter current and the boundary current are proportional to the inflow transport volume. This result corresponds well with NITANI's observation (1972, his Fig. 6), that a clear positive correlation exists between the maximum velocities of the Kuroshio and those of the KCC. Investigation of the governing equation further revealed that the width of the Kuroshio stream may widen as it protrudes onto the continental slope. However, this sloping western boundary does not significantly influence the pattern of the KCC.

From the numerical calculations, we also found that the planetary β -effect is essential in the formation of the branch current over the continental shelf. Unlike on an f -plane of reference, a water column branching southerly on a β -plane of reference is one way (by decreasing the planetary vorticity) to compensate for the vortex tube stretching caused by the inflow current crawling over the slope. Moreover, our numerical calculations showed that the existence of Taiwan, which intercepts the isobaths of the continental slope at the southwest end, is another indispensable condition in the formation of the KBC. The interception of Taiwan plays the role of the "western boundary" on a plane of topographic β , intensifying the southward-branched flow north of Taiwan and causing it to intrude onto the continental shelf. In cases on the β -plane of reference, the branch current over the continental slope is further reinforced by the wave energy transported southwestward by the topographic Rossby waves. After the branch current intrudes onto the continental shelf, the distance it extends depends on the bottom inclination there.

Acknowledgements—the authors wish to express their thanks to Mr T. Toda for his help in processing the AVHRR satellite picture and to Drs A. Maeda and T. Yamashiro of Kagoshima University for their discussions. They are also grateful to the Japan Oceanographic Data Center for providing the GEK data and to the anonymous reviewers for their useful suggestions. The computations were performed on the FACOM M-382 and VP-100 computers at the Data Processing Center of Kyoto University. A part of this study was supported by the Grant-in-Aid 60420014 from the Ministry of Education, Japan.

REFERENCES

- FUJIWARA I. (1981) On the hydrographic conditions of the East China Sea. *Marine Science*, **13**, 264–270 (in Japanese).
- GUAN B. and H. MAO (1982) A note on circulation of the East China Sea. *Chinese Journal of Oceanology and Limnology*, **1**, 5–16.
- HUH O. K. (1982a) Satellite observations and the annual cycle of surface circulation in the Yellow Sea, East China Sea and Korea Strait. *La Mer*, **20**, 210–222.
- HUH O. K. (1982b) Spring season flow of the Tsushima Current and its separation from the Kuroshio: Satellite evidence. *Journal of Geophysical Research*, **87**, 9687–9693.
- ICHIYE T. (1984) Some problems of circulation and hydrography of the Japan Sea and the Tsushima Current. In: *Ocean hydrodynamics of the Japan and East China Sea*, T. ICHIYE, editor, Elsevier, Amsterdam, pp. 15–54.
- INOUE N. (1981) Progress review on the hydrographic condition in the East China Sea. In: *Natural history of the Goto Islands, Japan—Comparison with Iki and Tsushima Islands*, A. YAMAMOTO, editor, Biological Society of Nagasaki Prefecture, pp. 29–72 (in Japanese).
- LEBLOND P. H. and L. A. MYSAK (1978) *Waves in the ocean*, Elsevier, Amsterdam, 602 pp.
- KONDO M. and K. TAMAI (1975) On the currents in the East China Sea. *Marine Science*, **7**, 27–33 (in Japanese).
- MINATO S. and R. KIMURA (1980) Volume transport of the western boundary current penetrating into a marginal sea. *Journal of the Oceanographic Society of Japan*, **36**, 185–195.
- NITANI H. (1972) Beginning of the Kuroshio. In: *Kuroshio—its physical aspects*, H. STOMMEL and Y. YOSHIDA, editors, Tokyo University Press, pp. 129–163.
- PEDLOSKY J. (1979) *Geophysical fluid dynamics*, Springer-Verlag, New York, 624 pp.